Prism-coupled light emission from tunnel junctions containing interface roughness: Experiment

J. Watanabe, A. Takeuchi, Y. Uehara, and S. Ushioda
Research Institute of Electrical Communication, Tohoku University, 2-1-1 Katahira, Sendai 980, Japan
(Received 25 April 1988)

We have measured the light-emission characteristics of Al–Al oxide–Au tunnel junctions that contain residual interface roughness, and compared them with the results of a theory we have just developed [Takeuchi, Watanabe, Uehara, and Ushioda, preceding paper, Phys. Rev. B (to be published)]. The tunnel junctions were formed on a glass substrate, which is attached to a coupler prism. The light-emission intensities were measured as a function of the emission angle and energy, through the prism and on the vacuum side. The theory can fit the emission-angle dependence almost exactly for a reasonable size of roughness. It can also fit the general features of the energy spectra, but some improvements are needed to achieve perfect agreement in detail. Several avenues for further refinements are suggested.

I. INTRODUCTION

Light emission from metal-oxide-metal tunnel junctions is interesting in terms of the physics of emission mechanisms and also from the viewpoint of possible applications as a means of light generation. These junctions consist of a substrate (usually glass), an Al film, an Al oxide barrier, and a counterelectrode which is usually made of metals like Au, Ag, and Cu. It is remarkable that such a simple device can emit visible light.

As the original discoverers of this phenomenon, Lambe and McCarthy[1] have correctly pointed out that surface plasmons and surfaces roughness play important roles in generating external light. In the past decade many groups worked on this problem through both experimental and theoretical methods.[2] Now the light-emission process from tunnel junctions is known to occur via two main steps: (1) generation of surface plasmons (electromagnetic normal modes of the junction structure) by the tunneling currents; (2) decay of surface plasmons into external light. The surface plasmon on a perfectly smooth surface is nonradiative, because its wave vector along the surface is always greater than that of the light of the same frequency. Thus it cannot couple directly to external light. Several different ways to induce surface plasmons to couple with and decay into light have been devised. One method is to make the junction surface randomly rough, thus breaking the wave-vector conservation rule parallel to the surface. This is the method used in their original experiment by Lambe and McCarthy. The second method is similar to this, but one places fine particles of metal between the oxide barrier and the top electrode. This method was used by Adams *et al.*[3] The third method was devised by Kirtley *et al.*[4] who formed the tunnel junction on a grating substrate. In these three methods the translational invariance of the surface is broken, resulting in the breakdown of wave-vector conservation. In the fourth method used by Ushioda *et al.*,[5] one places a coupler prism in contact with the tunnel junction. Here the wave vector of light in the prism is increased by a factor of the refractive index (n_p) of the prism, and the surface plasmon can decay into light conserving the wave vector.

An important feature of the coupler prism method is that the junction geometry is completely defined, because it does not involve surface roughness which is difficult to determine experimentally. Thus it was hoped that a complete theoretical analysis of the emission process can be carried out using smooth junctions. However, a theory of prism-coupled light emission from a completely smooth junction[6] could not explain the experimental results because of the presence of residual surface roughness, which affects the angular distribution and the spectrum of emission.

The previous theoretical paper by Takeuchi *et al.*[7] (paper I) deals with prism-coupled emission in the presence of surface roughness. The main purpose of the present paper is to describe the experimental results on nominally smooth junctions with residual roughness, which are treated in paper I, to make detailed comparisons with the predictions of the theory, and finally to determine its limits.

This paper is organized in the following sequence. Section II describes the method used in forming the tunnel junctions, and Sec. III describes the attenuated-total-reflection (ATR) measurements made to determine the film thicknesses and dielectric constants. In Sec. IV we describe the details of light-emission measurements as a function of the angle and energy. The results are compared with the theory in Sec. V. Section VI is the conclusion.

II. JUNCTION FABRICATION

The tunnel junctions were made by evaporation of metal films on a substrate of microscope cover glass in a vacuum jar at an approximate pressure of 3×10^{-6} torr. The cover glass was first washed by neutral detergent to remove dust and greasy materials, and then repeatedly cleansed using ethanol and acetone in an ultrasonic cleaner. Finally it was in ion free pure water. We found it very important to insure cleanliness of the substrate,

TABLE I. Comparison film thicknesses obtained by the ATR and quartz gauge methods. Also given are complex dielectric constants used as fitting parameters.

	Layer	Thickness (nm) Quartz gauge	Thickness (nm) ATR	ϵ_R	ϵ_I
Junction 1	Al	16.0	22.0	−43.0	17.5
	oxide		3.5	3.1	0.0
	Au	20.0	24.5	−10.0	1.70
Junction 2	Al	31.0	37.5	−44.0	17.0
	oxide		3.5	3.1	0.0
	Au	19.5	25.3	−10.9	1.53

particularly with respect to dust particles, in order to make successful junctions.

The Al film was deposited by thermal evaporation of 99.99% pure Al wire wrapped on a tungsten filament. The evaporation rate was monitored by a quartz thickness gauge and was kept in the range 1.5–2.0 nm/sec. The film thickness was in the range 20–30 nm.

The Al oxide barrier was formed either by keeping the sample out in clean air for about a day or by baking in an oven for about 10 min at 200–300 °C. As we see later, this procedure produces an oxide layer 2–3 nm thick.

After the barrier formation, the sample was placed in vacuum again, and a Au film was deposited. A Au wire of 99.99% purity was evaporated by heating in a Mo boat at the rate of 0.15–0.20 nm/sec. To form a successful junction, we found it necessary to maintain slow evaporation rate on this order. The thickness of the Au film was 20–30 nm similar to that of the Al film.

The Al and Au film strips were crossed over each other and had the dimensions 1×15 mm^2, resulting in a junction area of 1×1 mm^2. Copper wire electrodes were soldered on the metal strips using In solder. The typical resistance of the junction was around 50–100 Ω at the operating bias voltage. The tunnel junction is attached to a hemicylindrical coupler prism as illustrated in Fig. 1.

In this paper we present data from two of the junctions whose characteristics are given in Table I. Junction 1 was used to measure the emission from the prism side and junction 2 from the vacuum side. These junctions are not intended to be different, but it happened that clean data were obtained from different sides on the two junctions.

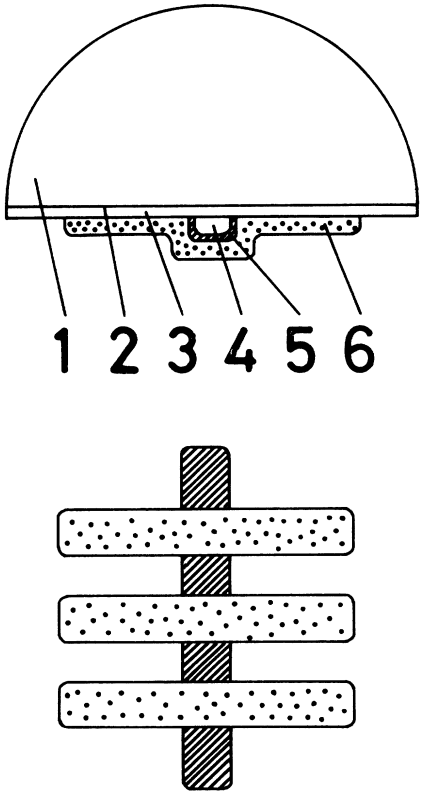

FIG. 1. Light-emitting tunnel junction pasted on the flat face of a hemicylindrical coupler prism; side and bottom views. (1), BK-7 coupler prism; (2), index matching oil; (3), microscope cover glass; (4), Al film; (5), Al oxide barrier; (6), Au film.

III. ATR MEASUREMENTS

In order to determine the film thicknesses and the dielectric constants of the metal and oxide layers, we measured the attenuated-total reflection (ATR) of the metal layers, first each layer separately and finally all layers together as a junction. The experimental setup for the ATR measurement is illustrated in Fig. 2.

The incident light was a beam from a He-Ne laser with the wavelength 632.8 nm at a power level of approxi-

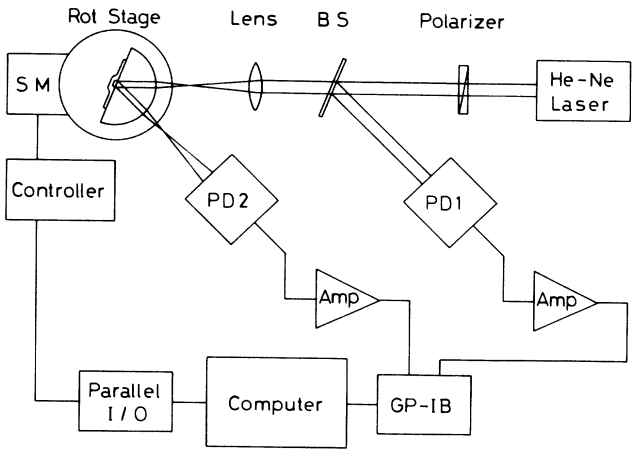

FIG. 2. Computer controlled ATR setup. BS, beam splitter; PD1, photodetector 1; PD2, photodetector 2; SM, stepping motor.

mately 0.5 mW. The microscope cover glass with the tunnel junction was pasted on the flat surface of a hemicylindrical prism made of borosilicate crown glass (BK-7) by an index matching oil. The prism is mounted on a rotating stage which can be turned by a stepping motor controlled by an NEC 9801VM computer. The beam splitter (BS) splits part of the beam into the photodetector PD1 which measures the incident intensity, and the reflected intensity from the sample is measured by the second photodetector PD2. The reflectivity was calculated from the ratio of the measured intensities by PD1 and PD2, and was recorded in a digitized form on a floppy disc as a function of the incident angle. Thus we measured the angle scan ATR.

Figure 3 shows the ATR of junction 1 for the Al-Al oxide layer, the Au layer, and the whole junction in that order from the top. The ATR of Al and Au layers was measured by shining the incident light slightly off the junction area where these metal strips do not overlap each other. The dots are the data points and the solid curves are the best fit curves derived from the theoretical expressions for each geometry.[8] The film thicknesses and the complex dielectric constants ($\epsilon_R + i\epsilon_I$) of the layers were determined by treating them as fitting parameters and finding the best fit. The resultant values are summarized in Table I. From Fig. 3 we see that an excellent fit can be achieved by these values of the parameters for individual layers as well as for the whole junction. The important point is that the three sets of data in Fig. 3 can be fitted with mutual consistency by a single set of parameters. Thus we believe that these values of film thicknesses and dielectric constants are reliable. Table I also allows comparison of film thicknesses obtained by the ATR method and by the quartz thickness gauge. The reading by the thickness gauge is consistently higher; we believe this results from the temperature variation of the quartz oscillator during evaporation. Thus we use the thicknesses obtained by the ATR method for subsequent calculations.

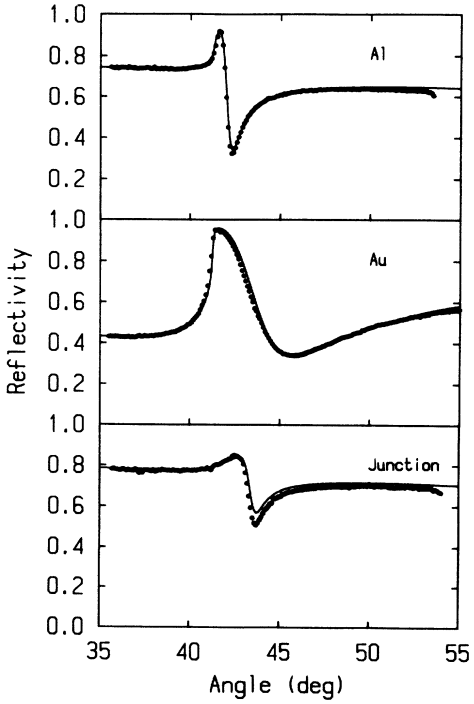

FIG. 3. ATR data; dots, measured reflectivity; curves, theoretical fit. Top panel, Al+oxide film; center panel, Au film; bottom panel, complete junction.

IV. EMISSION INTENSITY MEASUREMENTS

We measured the angle dependence and the energy dependence (emission spectra) of *s*- and *p*-polarized emission intensities from the prism side and the Au-vacuum side. The angle dependence was measured at a fixed energy (wavelength) of 2.07 eV (600 nm), and the energy dependence was measured at the emission angle of 43° from the normal where the intensity is peaked for *p*-polarized emission from the prism side.

The experimental setup for these measurements is shown in Fig. 4. The emission angle dependence was measured by setting the spectrometer at 600 nm and rotating the stage on which the tunnel junction with the coupler prism is fixed. The emission spectrum was measured by scanning the spectrometer with the rotation stage fixed at 43° emission angle on the prism side and 55° on the Au-vacuum side. All intensities were measured by photon counting, and digitized data were filed on a floppy disc. The relative sensitivity of the entire spectrometer-detector system was determined for *s* and *p* polarizations (with respect to the grating surface) by measuring the spectrum from a calibrated standard lamp. The data presented in the following discussions are corrected for the wavelength dependence of the relative sensitivity.

V. RESULTS AND COMPARISON WITH THEORY

Let us first discuss the angle dependence of emission. Figures 5 and 6 show the angle dependence of *p*- and *s*-polarized emissions, respectively, through the prism for junction 1. The applied bias voltage was 3.8 V and the measured current was 65 mA. The dots are the data

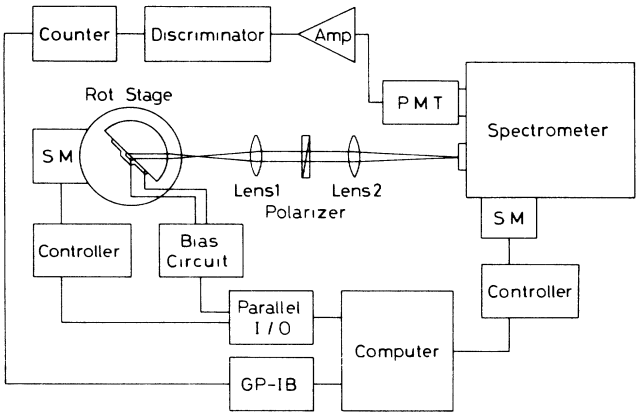

FIG. 4. Experimental setup for measuring emission intensities as a function of angle and energy.

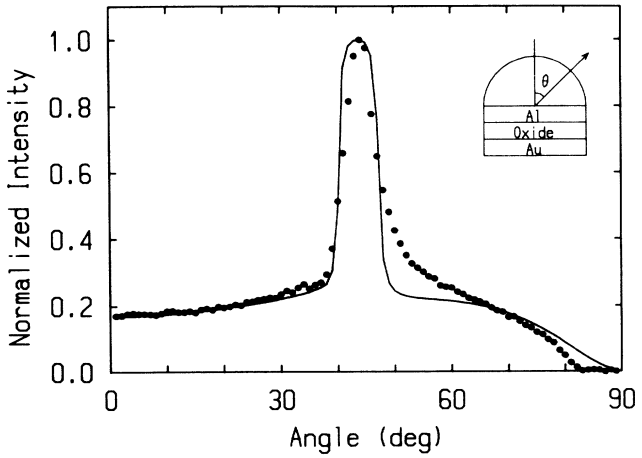

FIG. 5. Angle dependence of p-polarized emission intensity from junction 1 through the prism measured at 600 nm. Dots are the experimental data and the curve is the theoretical fit using the parameter values in Tables I and II. The vertical scale is normalized to unity at the experimental peak at 43°.

points and the solid curve is the calculated result from the theory of paper I. The intensity scale is normalized to unity at the experimental peak of Fig. 5, and the same normalization is used in Figs. 5, 6, and 9 for measurements on the prism side. Note the differences in the intensity calibrations on the vertical scale.

In Fig. 5 we see a peak at about 43° which arises from the emission by the fast mode. In addition there is a broad background over the entire angle range. This background should be absent if the junction is perfectly smooth. Also the s-polarized emission shown in Fig. 6 should be totally absent for a smooth junction.

The theoretical curves in Figs. 5 and 6 were calculated using the film thicknesses obtained by the ATR measurements, and the dielectric constants of Al, $-35.1+i11.6$ (Ref. 9), and Au, $-8.77+i1.37$ (Ref. 10). (Note that the values of the dielectric constants at 600 nm used here are different from the ones obtained by the ATR method at 632.8 nm.) We used the roughness parameters, the lateral correlation distance a, and the root-mean-square amplitude δ at each interface that are given in Table II. These values of a and δ were chosen to give reasonable fits to the eye. We assumed that there is no correlation between corrugated profiles at different interfaces. The special correlation distance ξ_0 for the current fluctuation (see paper I) was assumed to be 10 nm. The theoretical curves of Figs. 5 and 6 taken into account the effect of finite collection angle of the spectrometer which is ±3° about the center. Note in Fig. 5 that the broad background contribution is represented reasonably well by the theory that includes interface roughness. The strength of the broad background is mainly controlled by the roughness of the prism-Al interface. Thus in order to fit the intensity ratio between the top of the peak at 43° and the background, we had to assume a fairly large roughness amplitude at the prism-Al interface as indicated in Table II. (Note that the size of the roughness effect is proportional to the square of δ.) Thus by trying to fit the data in Fig. 5, we can fix the ratios among the roughness amplitudes for the four interfaces. As we have shown in paper I, the largest contribution to the emission intensity comes from the roughness at the metal-oxide interfaces.

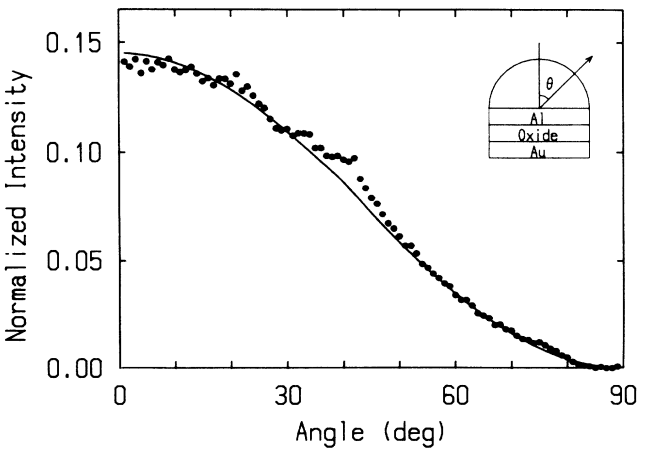

FIG. 6. Angle dependence of s-polarized emission intensity from junction 1 through the prism measured at 600 nm. Note the intensity scale which is common with that of Fig. 5.

The angle dependence of s-polarized emission is very well described by the same set of roughness parameters as seen in Fig. 6. The shape of the curve shown in Fig. 6 is not very sensitive to the choice of roughness parameters, so that this good agreement is not surprising. A slight bend in the data points noticeable around 43° can be fitted by the theoretical curve, if we make the relative size of the roughness at the Al-prism interface smaller. However, if we do so, the background-to-peak ratio in Fig. 5 cannot be reproduced properly.

The intensity ratio between the p- and s-polarized emission at the peak is 7.0:1 for the experimental data and the corresponding ratio from the theory is 6.7:1. This agreement indicates that the choice of the values for a and δ we made is reasonable.

The angle dependence of emissions on the Au-vacuum side is shown in Figs. 7 and 8 for p and s polarizations, respectively. These data were collected from junction 2. The range of collection angle was ±1°. The bias voltage and the current were typically 3.1 V and 66 mA, respectively. The intensity scales for Figs. 7, 8, and 10 for emission on the Au-vacuum side are all normalized at the experimental peak of Fig. 7 occurring around 60°. As we have indicated in Table II, we had to choose a large

TABLE II. Root-mean-square amplitude δ and lateral correlation distance a used in constructing theoretical curves.

	Interface	δ (nm)	a (nm)
Junction 1	Pr-Al	5	20
	Al Oxide	2	20
	Oxide Au	2	20
	Au Vacuum	2	20
Junction 2	Pr-Al	5	20
	Al Oxide	2	20
	Oxide Au	2	20
	Au Vacuum	10	20

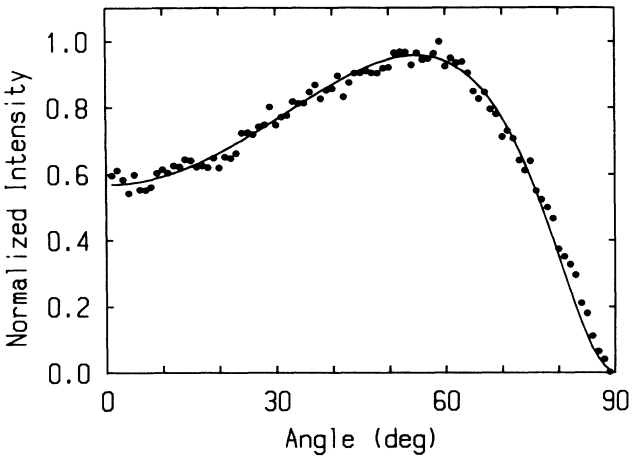

FIG. 7. Angle dependence of p-polarized emission intensity from junction 2 on the Au-air side measured at 600 nm. The intensity scale is normalized to the experimental peak around 60°.

root-mean-square roughness for the Au-vacuum interface in order to fit the experimental data of Fig. 7. If we choose the same values of roughness as for the curves in Figs. 5 and 6, the calculated curve will be too low near 0° corresponding to normal emission from the Au-vacuum side. Thus we chose 10 nm for the value of δ at the Au-vacuum interface. With this set of roughness values, the angle dependence for the s-polarized emission is well described as we see in Fig. 8. However, the value of $\delta = 10$ nm seems to be too large. The measured p- to s-polarization peak intensity ratio is 3.2:1, and the theory predicts 1.7:1.

In summary we may say that the angle dependence of emission from both sides of the junction is fairly well described by the present theory that includes the effect of interface roughness. Since both junctions 1 and 2 were made by identical procedures, we should expect similar characteristics for both of them with regard to interface roughness. However, we had to assume very large roughness at the Au-vacuum interface of junction 2, in order to fit the angle dependence of emission on the Au-vacuum side.

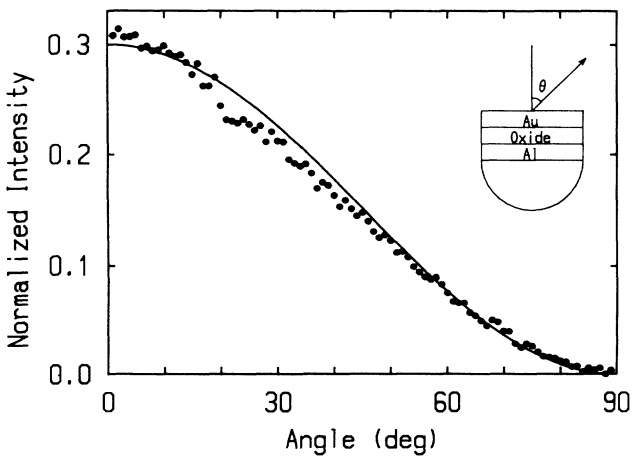

FIG. 8. Angle dependence of s-polarized emission intensity from junction 2 on the Au-air side measured at 600 nm. Note the intensity scale which is common with that of Fig. 7.

Now let us consider the emission spectra for a fixed emission angle. Figures 9 and 10 show the emission spectra for p and s polarizations from the prism side and the Au-vacuum side, respectively. The circles are the experimental data and the curves were drawn by applying the theory of paper I. The theoretical curves are averaged over the collection angles of the spectrometer in order to establish good correspondence with the experimental data. Again the data for the prism side was collected from junction 1 and for the Au-vacuum side from junction 2. The film thicknesses and the roughness parameters are the same as the ones used to calculate the angle dependence of emission given in Tables I and II. The frequency dependent dielectric constants for Al and Au were obtained by interpolation from Refs. 9 and 10, respectively.

In contrast to the good agreement obtained for the angle dependence, the emission spectra are only roughly represented by the theoretical curves as we see in Figs. 9 and 10. This fact is also reflected in the p-to-s intensity ratios at respective peaks. On the prism side, the experimental ratio is 10.3:1, while the theory predicts 10.5:1. On the Au-vacuum side, the measured ratio is 6.9:1, while the theoretical value is 5.4:1. (Note that the theoretical curves in each figure are drawn to show best fit to the eye, using different normalization constants.)

The data shown in Fig. 9 were collected with the bias voltage of 3.8 V. However, the emission intensity drops off rapidly around 2.3 eV, although weak emission is observed up to the energy corresponding to the bias voltage of 3.8 V. The theory reproduces this feature of the spectrum quite well. As was discussed in paper I, the asymptotic limit of the slow mode dispersion curve lies at about 2.2 eV. Thus we see that this drop in intensity corresponds to the cutoff of the slow mode. The presence of

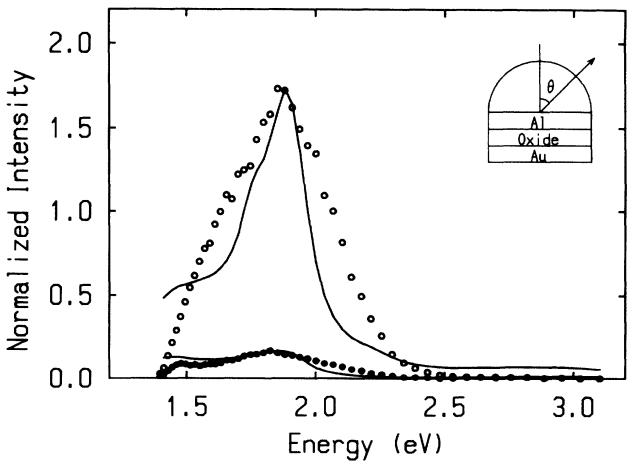

FIG. 9. Energy dependence of emission intensity from junction 1 through the prism, measured at 43° emission angle from the surface normal. Open circles, p polarization; solid circles, s polarization. The curves are the predictions of the theory using the parameters of Tables I and II. The intensity scale is common with that of Fig. 5. Bias voltage: 3.8 V.

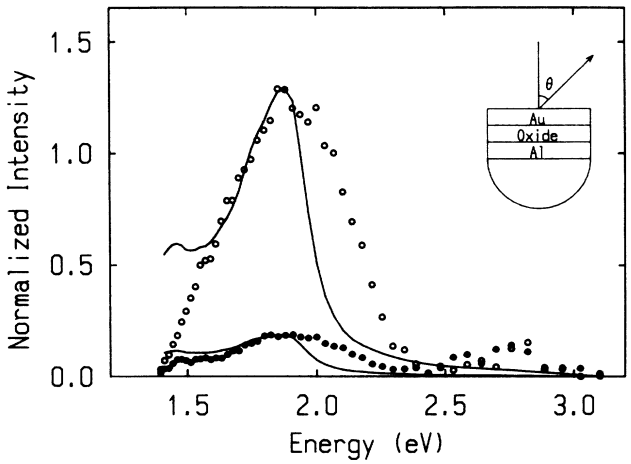

FIG. 10. Energy dependence of emission intensity from junction 2 on the Au-air side, measured at 55° emission angle from the surface normal. Open circles, *p* polarization; solid circles, *s* polarization. The intensity scale is common with that of Fig. 7. Bias voltage: 3.1 V.

the cutoff in the observed data is a clear indication that the main contribution to the emission intensity arises from the decay of the fast mode generated by conversion of the slow mode via interface roughness.

We found that the energy of the emission peak and the sharp dropoff is a fairly sensitive function of the thickness of the oxide layer. This fact can be understood easily, when we realize that the asymptotic limit of the slow mode depends sensitively on the oxide thickness. If the oxide thickness is very large, there are two surface-plasmon modes located on the two interfaces of the oxide layer with the adjacent metals, and these modes have similar frequencies independent of the oxide thickness. Since the actual oxide thickness is very small, the dispersion curves of these two branches repel each other. What has been called the slow mode is the lower of these two branches. Consequently, the slow mode dispersion curve is depressed when the oxide thickness is decreased. This is exactly what we found when we varied the oxide thickness; i.e., the emission peak and the sharp cutoff move down in energy when the oxide thickness is decreased. In fact we decided on the oxide thickness of 3.5 nm by varying it until we found the best fit to these features of the emission spectra. This procedure was necessary, because the ATR is insensitive to small changes in the oxide thickness. We plan to actually measure the oxide thickness using secondary-ion mass spectroscopy when this facility becomes available to us in the near future.

In spite of obvious mismatches seen in Figs. 9 and 10, there are some fine details where the observed spectra and the theoretical curves show matching features. For instance, notice the shoulder around 1.8 eV seen in the *p*-polarized spectrum in Fig. 9. This feature is also seen in the theoretical curve. Also a small peak seen around 1.5 eV in the *s*-polarized spectrum appears in the theoretical curve.

In summary the energy spectra are not precisely represented by the theory, but there is a general agreement on overall features as well as some of the fine details. Fitting of the energy spectra is much harder than fitting of the angle dependence, because the frequency dependence of the dielectric constants of the two metals is folded in the spectra. Thus some parts of the mismatch must arise from the dielectric constants. Unfortunately, there are disagreements in the fine details of the frequency dependent dielectric constants in the available literature. To correct this situation, we are planning to carry out frequency scanned ATR measurements to determine the dielectric constants of Al and Au films *in situ*.

Another likely source of error is in the frequency dependence of the Fourier transform of the current-current correlation function $J(\mathbf{Q}_p,\omega|zz')$, as we noted in paper I. Many simplifying assumptions are involved in arriving at the form of $J(\mathbf{Q}_p,\omega|zz')$ that was used in our calculations. Most likely, we must reexamine the details of this function, in order to predict the energy spectra correctly. In fact the form of this function is the most basic and yet the loosest end of the theory. We must also consider hot-electron scattering process which involves direct scattering of electrons with fast modes in the Au layer,[11] particularly for emissions on the Au-vacuum side. At present it is not clear how these processes should be incorporated in the expression for $J(\mathbf{Q}_p,\omega|zz')$.

From the level of agreements we have obtained between experiment and theory in this work, we believe that the theory presented in paper I correctly reflects the basic nature of light-emitting tunnel junctions with small interface roughness. The basic assumptions underlying this theory are the same as those used by Laks and Mills,[12] although some significant improvements are incorporated in paper I. Earlier difficulties encountered by Laks and Mills in matching the results of Adams *et al.*[3] was due partially to oversimplification of the junction geometry (assuming infinite thickness for the Al film and roughness only on the top surface, for instance), but we believe that the main cause was the size of the roughness of the junction. The junction used by Adams *et al.* contained Au balls whose size is too large to be within the limit of the first-order perturbation theory,[13] while our junctions contain only naturally occurring small residual roughness.

VI. CONCLUSION

We have made light-emitting tunnel junctions consisting of glass, Al, Al oxide, and Au that contain only residual interface roughness, and measured the emission intensities as a function of the emission angle and energy on the glass side through the coupler prism and into air on the other side of the junction. The emission-angle dependence on both sides agrees quite well with the prediction of the theory. On the other hand, the emission spectra can be fitted only in overall shapes. In order to fit the energy spectra, we need to determine the frequency dependence of the dielectric constants of the metals more precisely, and also to reexamine the frequency spectrum of the tunneling current fluctuations.

ACKNOWLEDGMENTS

We would like to acknowledge valuable interactions with J. E. Rutledge, P. D. Sparks, D. L. Mills, R. M. Pi-

erce, and J. Giergiel. These interactions were made possible by financial support from the Japan-U.S. Scientific Cooperation Program of the Japan Society for Promotion of Science and the U.S. National Science Foundation. We also wish to thank Murata Science Foundation and Toray Science Foundation for financial assistance. This work would not have been carried out so efficiently without the technical support and cooperation by the staff of the machine shop of our Institute.

[1]J. Lambe and S. L. McCarthy, Phys. Rev. Lett. **37**, 923 (1976).

[2]A good set of references is found in the reference section of P. Dawson, D. G. Walmsley, H. A. Quinn, and A. J. L. Ferguson, Phys. Rev. B **30**, 3164 (1984).

[3]A. Adams, J. C. Wyss, and P. K. Hansma, Phys. Rev. Lett. **42**, 912 (1979).

[4]J. R. Kirtley, T. N. Theis, and J. C. Tsang, Appl. Phys. Lett. **37**, 435 (1980).

[5]S. Ushioda, J. E. Rutledge, and R. M. Pierce, Phys. Rev. Lett. **54**, 224 (1985).

[6]S. Ushioda, J. E. Rutledge, and R. M. Pierce, Phys. Rev. B **34**, 6804 (1986).

[7]A. Takeuchi, J. Watanabe, Y. Uehara, and S. Ushioda, preceding paper, Phys. Rev. B **38**, 12 948 (1988).

[8]K. Kurosawa, R. M. Pierce, and S. Ushioda, Phys. Rev. B **33**, 789 (1986).

[9]M. A. Ordal, L. L. Long, R. J. Bell, S. E. Bell, R. R. Bell, R. W. Alexander, Jr., and C. A. Wood, Appl. Opt. **22**, 1099 (1983).

[10]P. B. Johnson and R. W. Christy, Phys. Rev. B **12**, 4370 (1972).

[11]J. R. Kirtley, T. N. Theis, J. C. Tsang, and D. J. DiMaria, Phys. Rev. B **27**, 4601 (1983).

[12]B. Laks and D. L. Mills, Phys. Rev. B **20**, 4962 (1979).

[13]K. Arya and R. Zeyher, Phys. Rev. B **28**, 4080 (1983).